AIAA JOURNAL
Vol. 31, No. 2, February 1993

Helicopter Trim Analysis by Shooting and Finite Element Methods with Optimally Damped Newton Iterations

N. S. Achar* and G. H. Gaonkar†
Florida Atlantic University, Boca Raton, Florida 33431

Helicopter trim settings of periodic initial state and control inputs are investigated for convergence of Newton iteration in computing the settings sequentially and in parallel. The trim analysis uses a shooting method and a weak version of two temporal finite element methods with displacement formulation and with mixed formulation of displacements and momenta. These three methods broadly represent two main approaches of trim analysis: adaptation of initial-value and finite element boundary-value codes to periodic boundary conditions, particularly for unstable and marginally stable systems. In each method, both the sequential and in-parallel schemes are used, and the resulting nonlinear algebraic equations are solved by damped Newton iteration with an optimally selected damping parameter. The impact of damped Newton iteration, including earlier-observed divergence problems in trim analysis, is demonstrated by the maximum condition number of the Jacobian matrices of the iterative scheme and by virtual elimination of divergence. The advantages of the in-parallel scheme over the conventional sequential scheme are also demonstrated.

Nomenclature

a = lift curve slope
C_d = resultant profile drag force in the plane of the rotor disk opposite to the flight direction
C_{d0} = profile drag coefficient
C_l = rolling moment coefficient
C_m = pitching moment coefficient
C_t = thrust coefficient
C_w = weight coefficient of the helicopter
C_φ = blade pitching-moment coefficient
$\boldsymbol{c}$ = control-input vector
F_β, F_ζ = aerodynamic moment per unit length of the blade in flap and lag directions, respectively
$\bar{f}$ = equivalent flat plate area of parasite drag
$g(s)$ = objective function to be minimized
H = Hamiltonian
$[I]$ = identity matrix
J = Jacobian or nondimensional torsional inertia
L = Lagrangian
P_β = flap natural frequency, rotating
p = generalized momentum, $L_{\dot{q}}$
Q = nonconservative force
q = generalized coordinate
R = rotor radius
s = state vector y augmented with control-input vector $\boldsymbol{c}$
T = kinetic energy
t_0, t_f = initial and final times
V = flight speed or potential energy
W = work done by Q
y = state vector
$y(t; y_0)$ = $y(t)$ with initial condition $y(0) = y_0$
α_s = shaft tilt angle
β = flap response
γ = lock number (blade inertia parameter)
ζ = lag response
θ = pitch angle, $\theta_0 + \theta_c \cos\psi + \theta_s \sin\psi$
θ_0, θ_c, θ_s = collective, longitudinal cyclic, and lateral cyclic pitch angles, respectively
λ = Newton damping parameter
λ_i = inflow
μ = advance ratio, $V \cos\alpha_s/\Omega R$
$\bar{\mu}$ = dimensionless flight speed, $V/\Omega R$
ξ = Newton direction, see Eqs. (4) and (5)
σ = rotor solidity
ψ = azimuth angle
Ω = rotor speed
ω_β, ω_ζ, ω_φ = dimensionless nonrotating flap, lag, and torsional natural frequencies
$[\,]^t$ = transpose of $[\,]$
$\| \ \|$ = vector norm
∇g = gradient of g
$(\,)$ = time derivative of $(\,)$
$(\,)_q$ = partial derivative of $(\,)$ with respect to q; similarly, subscripts p, q, $\dot{q}$, c, and y indicate partial differentiation

Received Nov. 25, 1991; revision received June 3, 1992; accepted for publication July 13, 1992.
*Graduate Student.
†Professor.

Introduction

THE helicopter trim settings comprise control inputs for required flight conditions and the corresponding initial conditions for periodic response. They are prerequisite for stability and vibration studies. The control inputs are specified indirectly so as to satisfy flight conditions of prescribed thrust levels, rolling and pitching moments, etc. In addition to the nonlinearity of the system and control-input equations, the control inputs appear not only in the system damping and stiffness matrices but also in the input matrix, and must be found concomitantly with the periodic response. The prediction of trim settings has been vigorously pursued since the 1980s and still is a demanding exercise because of divergence of iterative schemes and excessive machine time (Refs. 1–6).

Particularly, for marginally stable and unstable systems, the shooting method is increasingly used (e.g., 2GCHAS, Ref. 7); however, much recent research has been centered on temporal finite element methods of different versions, such as displacement, mixed and bilinear formulations, with further classifications in each of these formulations involving h, p, and hp versions.[4,5,8,9] No matter which method is used, computation of trim settings leads to nonlinear algebraic and transcendental equations, whose solution at present cannot be based on solid theory.[10] In fact, the computational difficulties of these equations virtually preclude the translation of several trim analysis methods into robust algorithms with global or reasonably qualified convergence characteristics. Little information is available on the nature of such difficulties or on ways to

quantify and alleviate them. Newton's method is the most widely used and perhaps the best method of solving nonlinear equations.[10] But although it guarantees quadratic convergence (the number of significant or accurate digits doubles after each iteration), it guarantees only local convergence and is sensitive to the initial guesses or starting values. Even with good starting values, the method can exhibit erratic divergence due to numerical corruption.[1]

The present investigation covers this divergence problem with respect to the shooting and two temporal finite element methods, which typify broadly two classes of methods: adaptation of time-marching methods of initial-value problems and finite element methods of boundary-value problems to periodic boundary conditions. It also covers the in-parallel scheme or the simultaneous computation of initial conditions and control inputs vis-a-vis the sequential scheme,[2] in which the iterations for the initial conditions and control inputs are carried out as two separate computational blocks, one following the other.[1,2] It must be emphasized that the divergence problem is not peculiar to the in-parallel scheme. In fact, it is as much a part of the sequential scheme. Moreover, the bulk of the earlier trim analysis investigation uses sequential computation. An exception is Ref. 1, which found appreciable machine time saving through the in-parallel scheme in the shooting method. However, that finding is masked by erratic divergence of Newton iteration.

Given this background, the present investigation is noteworthy in the following respects.

1) The Newton damping parameter is examined concerning both its selection (with a rational basis of minimizing an objective function) and its role in alleviating the sensitivity of Newton iteration to the starting values in the solution of trim settings of initial state and control inputs.

2) The computational reliability of the Newton iteration without and with optimal damping is quantified by the condition number of the Jacobian matrix, which also explains rationally the earlier-observed divergence problems.[1]

3) Concerning divergence and machine time, a comprehensive comparison of the sequential and in-parallel schemes is provided; each scheme is treated with Newton iteration both without and with damping. This exercise includes three trim analysis methods, representing two main approaches of trim analysis, particularly in stability investigations.

Damped Newton Method

The method retains the highly attractive features of the original Newton method (e.g., quadratic convergence) and yet almost global convergence.[10] We consider the solution of n nonlinear equations

$$f_i(s_1, s_2, \ldots, s_n) = 0; \qquad i = 1, 2, \ldots, n \tag{1}$$

or, in equivalent form,

$$f(s) = 0 \tag{2}$$

for which the Jacobian matrix is given by

$$J(s) = \frac{\partial f}{\partial s} = \frac{\partial f_i}{\partial s_j}; \qquad i, j = 1, 2, \ldots, n \tag{3}$$

The algorithm begins with the *"improved"* solution

$$s^{m+1} = s^m + \lambda\xi \tag{4}$$

where m is the iteration counter, λ is the *"optimal"* damping factor, and ξ is the solution of the linear system,

$$\xi = -J(s)^{-1} f(s) \tag{5}$$

The terms improved and optimal are qualified in the absence of a solution s^* such that $f(s^*) = 0$ and of optimality conditions to determine λ. The theory of unconstrained minimization and weak line search[10,11] provides a rational basis of quantifying these two terms and solving for the damping factor. We bypass the mathematical details and include instead a brief account of the method, following Ascher et al.[10]

The term s^{m+1} is an improvement over s^m in the sense of minimizing an associated objective function $g(s^m + \lambda\xi)$ monotonically, where

$$g(s) = 0.5 \sum_{i=1}^{n} f_i(s)^2 \tag{6}$$

The objective function has the property that $g(s) > 0$ and $g(s^*) = 0$ when $f(s^*) = 0$. Thus, the minimum of $g(s)$ provides the solution. Moreover, the Newton direction is a descent direction; that is, for the gradient ∇g, we have

$$\xi^t \nabla g = -[J^{-1} f]^t [J^t f] \tag{7a}$$

$$= -f(s)^2 = -2g < 0 \tag{7b}$$

Expanding $g(s + \lambda\xi)$, we obtain

$$g(s^m + \lambda\xi) = g(s^m) + \lambda\xi^t \nabla g(s^m) + \mathcal{O}(\lambda^2 |\xi|^2) < g(s^m) \tag{8}$$

where ∇g, which is equal to $J^t f$, shows that minimization is sought in the Newton's direction. Thus s^{m+1} is an improvement over s^m in the sense that

$$g(s^{m+1}) = g(s^m + \lambda\xi) < g(s^m) \tag{9}$$

which says that the solution s^* is keyed to the generation of monotonically decreasing values of $g(s)$.

We define from Eq. (8)

$$\varphi(\lambda) = \frac{g(s^m + \lambda\xi) - g(s^m)}{\lambda\xi^t \nabla g(s^m)} \tag{10}$$

The algorithm[10,11] makes use of a fixed parameter σ such that

$$0 < \sigma < 0.5 \tag{11a}$$

$$\sigma \le \varphi(\lambda) \le (1 - \sigma) \tag{11b}$$

From Eqs. (8) and (11), we have

$$[1 - 2\lambda(1 - \sigma)] g(s^m) \le g(s^{m+1}) \le (1 - 2\lambda\sigma) g(s^m) \tag{12}$$

The role of σ is sketched in Fig. 1, which shows the inherent predictor-corrector structure of the algorithm.[10] For the mth

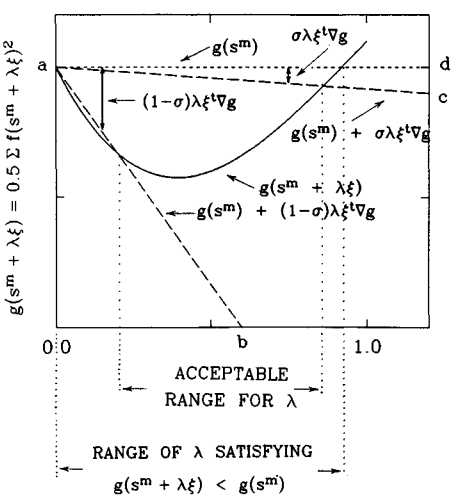

Fig. 1 Acceptable range of the damping parameter λ for the damped Newton iteration.

iteration counter, we approximate the scalar objective function by a quadratic:

$$g(s^m + \lambda\xi) \approx a\lambda^2 + b\lambda + c = \psi(\lambda) \tag{13}$$

where the three unknown constants—*a, b,* and *c*—are determined from the following conditions:

$$\psi(0) = g(s^m) \tag{14a}$$

$$\psi(\lambda_m) = g(s^m + \lambda_m\xi) \tag{14b}$$

$$\psi'(0) = \frac{\mathrm{d}}{\mathrm{d}\lambda}(s^m + \lambda\xi)\Big|_{\lambda=0} = \xi^t \nabla g(s^m) \tag{14c}$$

The criterion that $\psi(\lambda)$ is a minimum with respect to λ can be expressed as

$$\lambda = \frac{-\lambda_m^2\psi'(0)}{2[\psi(\lambda_m) - \psi(0) - \lambda_m\psi'(0)]} \leq \frac{\lambda_m}{2(1-\sigma)} \tag{15}$$

The preceding algorithm has been found to work generally well[10]; direct computational experience in computing trim settings supports this as well. However, there are cases of the algorithm breaking down when the objective function fails to decrease monotonically. That is, when $g(s)$ has local minima and/or singularities, Eq. (13) may not be a good approximation to $g(s)$. Hence, the algorithm fails to compute λ satisfying Eq. (9). This problem has been alleviated as follows. At the end of every iteration, before computing the damping parameter λ, $s^{m+1} = s^m + \lambda\xi$ is computed with $\lambda = 1.0$. Then, if any of the control inputs in s^{m+1} exceeds physically realistic values (say shaft tilt $\alpha_{s,\max} = 20$ deg), an upper limit for λ, λ_m, is chosen such that the control inputs in s^{m+1} are physically realistic. Then the algorithm proceeds to find optimum λ in the range 0 to λ_m as before. Again, in extreme cases if the algorithm fails to find λ satisfying monotonicity Eq. (9), λ_m itself is chosen as the optimum λ. Though the monotonic decrease in $g(s)$ is not guaranteed with $\lambda = \lambda_m$, the algorithm converges to the trim settings, which are elaborated on later with the help of numerical results.

Condition Number of *J*

The relative error in the solution of trim equations by Newton iteration can be bound by utilization of the condition number of the Jacobian matrix, cond(J), which also quantifies the robustness of the Newton direction; see Eq. (5). To provide an improved appreciation of the role of cond(J), we emphasize that the *actual* computation of trim equations does not follow Eq. (5); it follows a numerically perturbed equation:

$$[J + \delta J]\{\xi + \delta\xi\} = \{f + \delta f\} \tag{16a}$$

The following inequality[12]

$$\frac{\|\delta\xi\|}{\|\xi\|} < \mathrm{cond}(J)\left[\frac{\|\delta J\|}{\|J\|} + \frac{\|\delta f\|}{\|f\|}\right] \tag{16b}$$

shows that cond(J) represents the maximum possible magnification of the sum of relative errors in J and f. Thus, the higher the value of cond(J), the greater the sensitivity of Eq. (16a) to computational perturbations and, consequently, the less well conditioned is the computational problem of finding the control inputs and periodic initial state.[13]

With the definition

$$\delta = \max[1/\mathrm{cond}(J)] \tag{17}$$

and with Eqs. (3–7), it can be shown that[10]

$$\delta\,|\nabla g|\,|\xi| = \delta\,|J^t f|\,|J^{-1} f| \leq |f|^2 = -\nabla g^t \xi \tag{18}$$

Equations (5) and (18) show that, with increasing value of cond(J), the overall conditioning of the Newton direction decreases. That is, the product $\nabla g^t \xi$ decreases, although the correction $|\xi|$ is not small and $g(s)$ does not decrease rapidly along the Newton direction ξ. Schematically stated, lines *ab* and *ac* tend to merge with line *ad* in Fig. 1.

Trim Formulation

We include a brief account of the shooting method[1] and the weak version of a temporal finite element method with mixed formulation[8] of displacements and momenta. The algorithmic details of the temporal finite element method with displacement formulation run similar to those of mixed formulations and are omitted here; for details see Ref. 4. This facilitates appreciation of the algorithmic aspects of sequential and in-parallel schemes of Newton iteration in the trim analysis by the shooting and finite element methods. For convenience, the latter two finite element methods of mixed and displacement versions are, respectively, represented as FEM-M and FEM-D. In the three methods, the algorithm follows the in-parallel scheme or the simultaneous computation of initial conditions and control inputs. The straightforward adaptation to the sequential scheme is not spelled out explicitly.

Shooting Method

In trim analysis, equations of motion in state variable form

$$\dot{y} = G[y(t), c] \tag{19}$$

satisfy the unknown periodic initial state y_0, that is,

$$y(2\pi; y_0) - y_0 = 0 \tag{20}$$

Further, the unknown control inputs c should be determined such that the desired flight conditions

$$f(y, c) = 0 \tag{21}$$

are satisfied. Equations (20) and (21) comprise the nonlinear algebraic trim equations, which are symbolically represented as Eq. (2), where $s = \lfloor y, c \rfloor^t$ is the augmented vector of trim settings. These equations are solved using Newton iteration to get the trim settings.

FEM-M

The Hamilton's law of varying action or HLVA of a system can be represented as

$$\delta \int_{t_0}^{t_f} (L + W)\,\mathrm{d}t - (L_{\dot{q}}\,\delta q)\Big|_{t_0}^{t_f} = 0 \tag{22}$$

in which the system is represented in configuration space in terms of the generalized coordinates. In the mixed formulation, we first represent Eq. (22) in terms of the coordinates from the phase space using the Hamiltonian of the system, such that both generalized displacement q and generalized momentum p become primary variables. By varying the Hamiltonian of the system,

$$H = H(q, p, t) = p.\dot{q} - L(q, \dot{q}, t) \tag{23}$$

we obtain

$$\delta H = \delta p.\dot{q} + p.\,\delta\dot{q} - \delta L(q, \dot{q}, t)$$

Hence,

$$\delta L = \delta p \cdot \dot{q} + p \cdot \delta\dot{q} - \delta H(q, p, t)$$

$$= \delta p \cdot \dot{q} + p \cdot \delta\dot{q} - (H_q \cdot \delta q + H_p \cdot \delta p)$$

Substituting for δL in Eq. (22), we have

$$\int_{t_0}^{t_f} [\delta p.\dot{q} + p.\delta\dot{q} - (H_q.\delta q + H_p.\delta p - Q\delta q)]\, dt = (p.\delta q)\Big|_{t_0}^{t_f} \tag{24}$$

In the previous equation, $\dot{q}$ occurs only in the first term. Hence, integrating the first term by parts, $\dot{q}$ can be eliminated from the previous equation to get

$$\int_{t_0}^{t_f} [-\delta\dot{p}.q + p.\delta\dot{q} - (H_q.\delta q + H_p.\delta p - Q\delta q)]\, dt = [(p.\delta q) - (q.\delta p)]\Big|_{t_0}^{t_f} \tag{25}$$

With the definition

$$y = \begin{Bmatrix} q \\ p \end{Bmatrix}, \quad \delta y = \begin{Bmatrix} \delta q \\ \delta p \end{Bmatrix}, \quad \hat{H} = \begin{Bmatrix} H_q - Q \\ H_p \end{Bmatrix}, \quad B = \begin{Bmatrix} p \\ -q \end{Bmatrix}$$

and

$$\begin{Bmatrix} p \\ -q \end{Bmatrix} = \begin{bmatrix} 0 & I \\ -I & 0 \end{bmatrix} \begin{Bmatrix} q \\ p \end{Bmatrix} = \hat{N}.y \tag{26}$$

Eq. (25) can be expressed in vectorial form:

$$\int_{t_0}^{t_f} (\delta\dot{y}.\hat{N}y - \delta y.\hat{H})\, dt = [\delta y.B]\Big|_{t_0}^{t_f} \tag{27}$$

When $\hat{H}$, defined in Eq. (26), is nonlinear in y, it can be linearized about a steady-state value $\bar{y}$ as

$$\hat{H} = \hat{H}(\bar{y}) + \hat{H}(\bar{y})_y \Delta y \tag{28}$$

where

$$\hat{H}(\bar{y}) = \begin{Bmatrix} H_q - Q \\ H_p \end{Bmatrix}, \quad \hat{H}(\bar{y})_y = \begin{bmatrix} H_{qq} - Q_q & H_{qp} - Q_p \\ H_{pq} & H_{pp} \end{bmatrix} \tag{29}$$

Substituting Eq. (28) in Eq. (27), we obtain

$$\int_{t_0}^{t_f} \{\delta\dot{y}.\hat{N}(\bar{y} + \Delta y) - \delta y\hat{H}(\bar{y}) - \delta y[H(\bar{y})_y]\Delta y\}\, dt = (\delta y.B)\Big|_{t_0}^{t_f} \tag{30}$$

Next, the time interval $[t_0, t_f]$ is discretized into m smaller segments; i.e., $t_0 = t_1 < t_2 < \ldots t_i \ldots < t_{m+1} = t_f$. In each of these temporal elements, the generalized coordinate q_e and the momentum p_e can be expressed in terms of some appropriate shape functions as follows.

Since the derivatives of q and p do not occur in Eq. (25), constant values with discrete end momenta and displacements will satisfy the completeness requirements[8]; i.e., we can have

$$y_e = \begin{Bmatrix} q \\ p \end{Bmatrix} = \begin{Bmatrix} \bar{q}_i \\ \bar{p}_i \end{Bmatrix} \quad \text{if} \quad t_i < t < t_{i+1}$$

$$y_e = \begin{Bmatrix} q_i \\ p_i \end{Bmatrix} \quad \text{if} \quad t = t_i; \qquad y_e = \begin{Bmatrix} q_{i+1} \\ p_{i+1} \end{Bmatrix} \quad \text{if} \quad t = t_{i+1} \tag{31}$$

However, the virtual displacement and the virtual momentum require piecewise differentiable functions.[8] Hence, we choose

$$\delta y_e = \begin{Bmatrix} \delta q \\ \delta p \end{Bmatrix} = \begin{bmatrix} (1-\tau) & 0 & \tau & 0 \\ 0 & (1-\tau) & 0 & \tau \end{bmatrix} \begin{Bmatrix} \delta q_i \\ \delta p_i \\ \delta q_{i+1} \\ \delta p_{i+1} \end{Bmatrix} = M\delta\hat{y}_e \tag{32}$$

with

$$\tau = \frac{(t - t_i)}{(t_{i+1} - t_i)}$$

Substituting for Δy and δy in Eq. (30) from Eqs. (31) and (32), respectively, for the ith time element, we have

$$\delta\hat{y}_e - \left[\int_{t_i}^{t_{i+1}} [\dot{M}^t.\hat{N}(\bar{y}_e + \Delta y_e) - M^t\hat{H}(\hat{y}) - M^t\hat{H}(\hat{y})_y\Delta y_e]\, dt - (M^tB)\Big|_{t_i}^{t_{i+1}}\right] = 0 \tag{33}$$

Defining

$$F_e = \int_{t_i}^{t_{i+1}} [M^t\hat{H}(\bar{y}) - \dot{M}^t.\hat{N}\bar{y}_e]\, dt$$

$$K_e = \int_{t_i}^{t_{i+1}} [M^t\hat{H}(\bar{y})_y - \dot{M}^t.\hat{N}]\, dt$$

and

$$G_e = (M^tB)\Big|_{t_i}^{t_{i+1}} = \begin{Bmatrix} -p_i \\ q_i \\ p_{i+1} \\ -q_{i+1} \end{Bmatrix}$$

Eq. (33) can be expressed as

$$\delta\hat{y}_e[F_e + K_e\Delta y_e + G_e] = 0 \tag{34}$$

Next, all of the m elemental Eqs. (34) are generated and assembled to get the global, linearized variational statement

$$\delta\hat{y}[F + K\Delta y + G] = 0 \tag{35}$$

where K, F, G, y, $\delta\hat{y}$ are the global stiffness matrix, force vector, momentum vector, displacement vector, and the virtual displacement vector, respectively. The elements of the vectors G, y, and $\delta\hat{y}$ are given next:

$$G = \lfloor -p_1, q_1, 0, \ldots, 0, 0, p_{m+1}, -q_{m+1} \rfloor^t \tag{36a}$$

$$y = \lfloor \bar{q}_1, \bar{p}_1, \bar{q}_2, \bar{p}_2, \ldots, \bar{q}_m, \bar{p}_m \rfloor^t \tag{36b}$$

$$\delta\hat{y} = \lfloor \delta q_1, \delta p_1, \delta q_2, \delta p_2, \ldots, \delta q_{m+1}, \delta p_{m+1} \rfloor^t \tag{36c}$$

Then, applying the periodic boundary conditions to Eq. (35) (i.e., $q_1 = q_{m+1}$ and $p_1 = p_{m+1}$), we get

$$\boldsymbol{F} + \boldsymbol{K}\Delta y = 0 \tag{37}$$

where $\boldsymbol{F}$ and $\boldsymbol{K}$ are F and K, respectively, rearranged after applying the boundary conditions. Next, Eq. (37) is solved using Newton iteration until the series $y = \Sigma\Delta y_i$ converges, both $\boldsymbol{F}$ and $\boldsymbol{K}$ being updated at the end of each iteration.

Parallel Trim Method

For the parallel solution of trim settings, we reformulate the $\boldsymbol{F}$ and $\boldsymbol{K}$ of Eq. (37) as follows. Since $\hat{H}$, defined in Eq. (26), is nonlinear in both y and c, it can be linearized about some mean position $\bar{y}$ and $\bar{c}$. (Note: the Hamiltonian H is nonlinear in q and p, and the generalized force Q is nonlinear both in p, q, and c.) That is,

$$\hat{H} = [\hat{H}(\bar{y}, \bar{c}) + \hat{H}(\bar{y}, \bar{c})_y\Delta y + \hat{H}(\bar{y}, \bar{c})_c\Delta c] \tag{38}$$

where

$$\hat{H}(\bar{y}, \bar{c})_c = \begin{bmatrix} H_{qc} & -Q_c \\ & H_{pc} \end{bmatrix}$$

and $\hat{H}(\bar{y}, \bar{c})_y = \hat{H}(\bar{y})_y$; see Eq. (29). Substituting Eq. (38) into Eq. (27), we get the variational statement for each element as

$$\delta y_e \left[\int_{t_i}^{t_{i+1}} [\dot{M}^t.\hat{N}(\bar{y}_e + \Delta y_e) - M^t\hat{H}(\bar{y}) - M^t\hat{H}(\bar{y})_y \Delta y_e - M^t\hat{H}(\bar{y}, \bar{c})_c \Delta c] \, dt - (M^tB)\Big|_{t_i}^{t_{i+1}} \right] = 0 \tag{39}$$

Defining

$$F_e = \int_{t_i}^{t_{i+1}} [M^t\hat{H}(\bar{y}, \bar{c}_y) - \dot{M}^t.\hat{N}\bar{y}_e] \, dt$$

$$K_e = \int_{t_i}^{t_{i+1}} [M^t\hat{H}(\bar{y}, \bar{c})_y - \dot{M}^t.\hat{N}] \, dt$$

$$K_{ec} = \int_{t_i}^{t_{i+1}} [M^t\hat{H}(\bar{y}, \bar{c})_c] \, dt$$

$$G_e = (M^tB)\Big|_{t_i}^{t_{i+1}} = \begin{Bmatrix} -p_i \\ q_i \\ p_{i+1} \\ -q_{i+1} \end{Bmatrix} \tag{40}$$

Eq. (39) can be represented as

$$\delta\hat{y}_e[F_e + K_e\Delta y_e + K_{ec}\Delta c + G_e] = 0 \tag{41}$$

Next, all of the elemental Eqs. (41) are generated and assembled to get the global, linearized variational statement

$$\delta\hat{y}[F + K\Delta y + K_c\Delta c + G] = 0 \tag{42}$$

Further, Eq. (21) can be linearized as

$$f(y, c) = f(\bar{y}, \bar{c}) + [f(\bar{y}, \bar{c})_y\Delta y + f(\bar{y}, \bar{c})_c\Delta c] = 0 \tag{43}$$

Now, Eqs. (42) and (43) are combined and the boundary condition is applied to get the augmented force vector and stiffness matrix, F and K of Eq. (37), respectively. Then, Eq. (37) is solved iteratively, until the augmented vector $s = \Sigma\Delta s_i$ converges where $\Delta s_i = \lfloor \Delta y_i, \Delta c_i \rfloor^t$.

Model Description

For computational purposes, flap-lag and flap-lag-torsion models are selected; both the models are based on quasisteady aerodynamics and rigid-body mode representation. However, for the simplicity of illustrating the algorithmic and computational aspects, model description and much of the discussion of numerical results are for the flap-lag model, which was also treated in Ref. 1 by the shooting method. We begin with the state vector $y(t)$ with four components comprising the flap angle β and lag angle ζ and their rates $\dot{\beta}$ and $\dot{\zeta}$: $y(t) = \lfloor \beta(t), \dot{\beta}(t), \zeta(t), \dot{\zeta}(t) \rfloor^t$. Part of the trim analysis is to compute the periodic initial state y_0 such that

$$y(2\pi; y_0) - y_0 = 0 \tag{44}$$

The remaining part of the trim analysis is to compute the four control parameters—three pitch angles θ_0, θ_s, θ_c and shaft tilt α_s—to satisfy the following four trim equations of force and moment balance:

$$C_t \cos(\alpha_s) + C_d \sin(\alpha_s) = C_w \tag{45}$$

$$C_t \sin(\alpha_s) - C_d \cos(\alpha_s) = 0.5\mu^2\bar{f} \tag{46}$$

$$C_l = 0 \tag{47}$$

$$C_m = 0 \tag{48}$$

The solution of four initial-condition equations, typified by Eq. (44), and four trim equations, Eqs. (45–48), constitutes the trim analysis. The nondimensional thrust C_t and horizontal force C_d depend on the total blade root shear forces: $\bar{F}_\beta$, normal to the blade in the flap direction; $\bar{F}_\zeta$, in the lag direction; and $\bar{F}_r$, in the outward radial direction. These shear forces are given by

$$\bar{F}_\beta = -1.5\ddot{\beta} - 1.5\cos(\beta)\sin(\beta)(1 + \dot{\zeta})^2 + \int_0^1 F_\beta \, dr \tag{49}$$

$$\bar{F}_\zeta = -1.5\ddot{\zeta}\cos^2(\beta) + 3\sin(\beta)\cos(\beta)(1 + \dot{\zeta})\dot{\beta} + \cos\beta\int_0^1 F_\zeta \, dr \tag{50}$$

$$\bar{F}_r = 1.5[(1 + \dot{\zeta})^2\cos^2(\beta) + \dot{\beta}^2] \tag{51}$$

Then, C_t and C_d, in Eqs. (45) and (46), and the rolling moment and the pitching moment coefficients, C_l and C_m, respectively, in Eqs. (47) and (48), are given by

$$\frac{C_t}{\sigma a} = \frac{1}{\gamma 2\pi}\int_0^{2\pi} [\bar{F}_\beta\cos(\beta) + \bar{F}_r\cos(\beta)] \, d\psi \tag{52}$$

$$\frac{C_d}{\sigma a} = \frac{1}{\gamma 2\pi}\int_0^{2\pi} [\bar{F}_\beta\sin(\beta)\cos(\psi + \zeta) + \bar{F}_\zeta\sin(\psi + \zeta) + \bar{F}_r\cos(\beta)\cos(\psi + \zeta)] \, d\psi \tag{53}$$

$$\frac{C_l}{\sigma a} = -\frac{(P_\beta^2 - 1)}{\gamma 2\pi}\int_0^{2\pi} \beta\sin(\psi + \zeta) \, d\psi \tag{54}$$

$$\frac{C_m}{\sigma a} = -\frac{(P_\beta^2 - 1)}{\gamma 2\pi}\int_0^{2\pi} \beta\cos(\psi + \zeta) \, d\psi \tag{55}$$

The final component of the trim analysis concerns the uniform total inflow λ_i:

$$\lambda_i = \mu\tan(\alpha_s) + C_t/[2\sqrt{\ }(\mu^2 + \lambda_i^2)] \tag{56}$$

which is solved iteratively in combination with C_t and α_s.

Trim Analysis Results

Trim analysis uses the shooting method and the two finite element methods, FEM-M and FEM-D. The control inputs and initial conditions are computed simultaneously as one block in the in-parallel scheme; they are computed sequentially as two separate blocks in the sequential scheme. Unless stated otherwise, the rigid flap-lag model with in-parallel scheme is used; nonlinear equations are solved by conventional Newton iteration with no damping, and the following baseline values are assumed: $\gamma = 5$, $\omega_\beta = 0.57$, $\omega_\zeta = 1.4$, $\sigma = 0.05$, $a = 6.28$, $C_w = 0.01$, $C_{d0} = 0.01$, $\bar{f} = 0.01$, and $0 \le \bar{\mu} \le 0.7$. The computations are performed on a VAX 6320. The sparse matrices obtained by the finite element methods are solved using the NAG subroutine (F01BRF), which considers the matrix sparsity.

In the finite element methods, it is first necessary to arrive at the number of elements (NEL) needed for the a priori specified level of tolerance in the solution of periodic response. This tolerance is further substantiated on the basis of a relative error norm criterion with the shooting-method results[1,2] as reference values. For that purpose, a typical flight speed, $\bar{\mu} = 0.4$, is chosen. As shown in Fig. 2a for a typical

initial state $\dot{\beta}(0)$, all of the periodic initial conditions, $y = \lfloor \beta(0), \dot{\beta}(0), \zeta(0), \dot{\zeta}(0) \rfloor^t$, converge as the number of elements increases. In particular, it was found that for asymptotic convergence of all of the four components of y, we need at least NEL = 12 for FEM-D and NEL = 16 for FEM-M. Concerning the minor differences between results from the three trim methods, the relative error norm in $y = \lfloor \beta, \dot{\beta}, \zeta, \dot{\zeta} \rfloor^t$, obtained by the respective FEM, is defined as

$$\text{Relative error norm} = \frac{1}{\text{NEL}} \sqrt{\left[\frac{\Sigma \| y_{\text{shoot}} - y_{\text{fem}} \|_i^2}{\Sigma \| y_{\text{shoot}} \|_i^2} \right]}$$

$$i = 1, \ldots, \text{NEL}$$

As seen from Fig. 2b, as the number of elements increases, the relative error norm decreases rapidly; for NEL = 12 for FEM-D and for NEL = 16 for FEM-M, the relative error norm is less than 0.01. For the previous NEL values selected on the basis of the results at $\bar{\mu} = 0.4$, it was also verified that right up to $\bar{\mu} = 0.7$ the relative error norm is less than 0.01. Thus, in summary, NEL values of 12 and 16 for FEM-D and FEM-M, respectively, guarantee 1) asymptotic convergence for $\bar{\mu} = 0.4$ and 2) a relative error norm of less than 0.01 for $0.0 \le \bar{\mu} \le 0.7$. Spot checks for other values of $\bar{\mu}$ show that asymptotic convergence with these NEL values holds for $0.0 \le \bar{\mu} \le 0.7$ as well. Overall, with these NEL values, the control inputs θ_0, θ_s, θ_c, and α_s and the periodic responses β, $\dot{\beta}$, ζ, and $\dot{\zeta}$ agree with the shooting method results. Hence, these NEL values are chosen in all of the subsequent numerical results with the flap-lag model. (This agreement is further elaborated later on for the flap-lag-torsion model.)

In Figs. 3–5, the machine times taken by the sequential and in-parallel schemes in the three trim analysis methods are presented. Given the sensitivity of Newton iteration to starting values, the results for each of the methods are presented for two sets of starting values. In Figs. 3a, 4a, and 5a, we use the *exact* solution of the preceding flight speed $\bar{\mu}$ as the starting value; the exact solution is taken as the one obtained by continuation approach with $\bar{\mu}$ as a continuation parameter and $\Delta\bar{\mu} = 0.05$ as the continuation step size. For example, starting values, say at $\bar{\mu} = 0.3$, are given by the solution at the preceding value of $\bar{\mu} = 0.25$. For a given flight speed, the cumulative

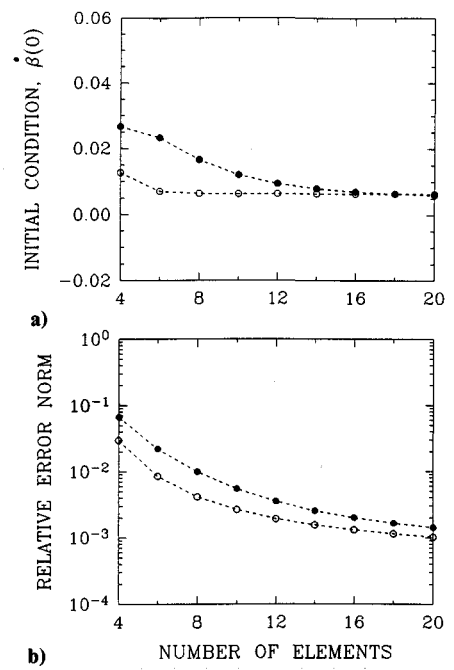

Fig. 2 Convergence of periodic initial condition in FEM-D and FEM-M with increasing number of elements at $\bar{\mu} = 0.4$ (∘----∘ FEM-D, •----• FEM-M).

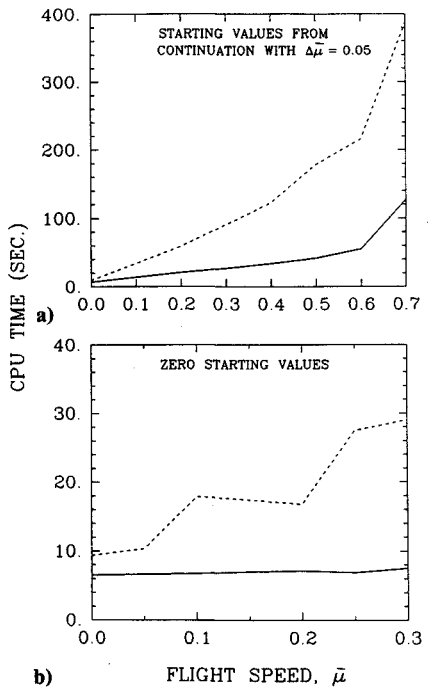

Fig. 3 Machine time comparison in the shooting method with sequential and in-parallel schemes (---- sequential, —— in-parallel).

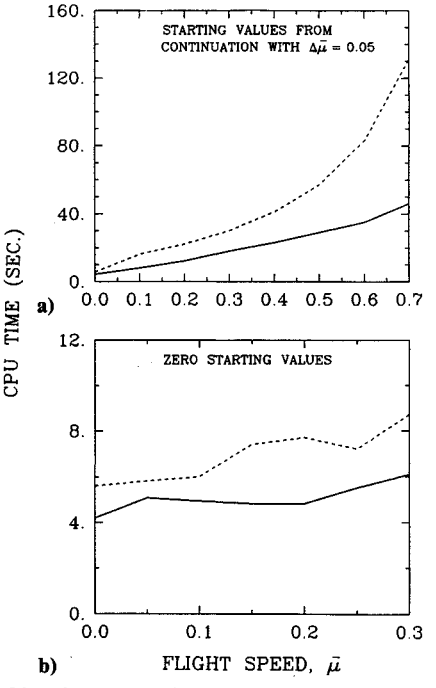

Fig. 4 Machine time comparison in the FEM-D with sequential and in-parallel schemes (---- sequential, —— in-parallel).

machine times taken starting from $\bar{\mu} = 0$ are shown in part a of Figs. 3–5. Though prohibitively costly, this approach to the starting values provides a rational basis of providing the *best* starting values. The other extreme is to begin with zero starting values, perhaps the most demanding starting values for the iteration. This is done in part b of Figs. 3–5; owing to the divergence problem of Newton iteration with zero starting values in both the sequential and in-parallel schemes, the results are limited to $\bar{\mu} \le 0.3$. Figures 3–5 show that the in-parallel scheme is more economical than the sequential scheme. This saving is observed for both sets of starting values (contin-

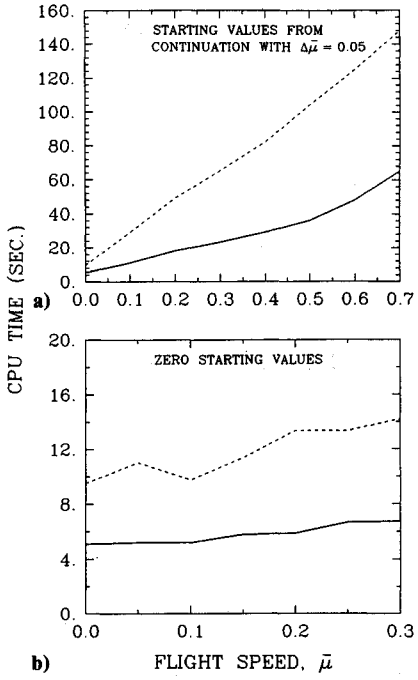

Fig. 5 Machine time comparison in the FEM-M with sequential and in-parallel schemes (---- sequential, —— in-parallel).

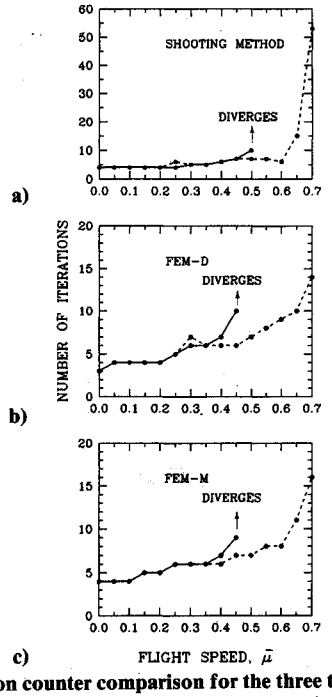

Fig. 6 Iteration counter comparison for the three trim analysis methods with zero starting values (—— without damping, ---- with damping).

uation with $\Delta\bar{\mu} = 0.05$ and zero starting values), showing that the in-parallel scheme is preferable regardless of the starting values.

The preceding results are based on Newton iteration with no damping, and mention is made of the divergence of the iteration with zero starting values. The impact of damped Newton iteration on divergence and related issues are pursued in Figs. 6-9; an important observation is that the damped Newton method did not encounter divergence. Figures 6 and 7 show the mechanism of divergence relative to iteration counter and the starting values. This is followed by Figs. 8 and 9, which show a means of quantifying and understanding divergence as well as computing the Newton damping parameter, which virtually eliminates divergence.

Figure 6 shows the iteration counter vs flight speed. Whereas iteration without damping experiences divergence for approximately $\bar{\mu} = 0.45$, damped iteration does not diverge, although its iteration counter increases with increasing $\bar{\mu}$. That the Newton damping parameter makes the iteration more controlled and "gives less room for erratic behavior"[10] is well borne out in Fig. 6. Also, for $\bar{\mu} > 0.6$ or so, the iteration counter in the damped iteration rapidly grows in the shooting method, indicating poor convergence. By comparison the damped iteration in FEM-M and FEM-D is remarkably smooth; the iteration counter and its growth with increasing $\bar{\mu}$ are much less rapid, and it hardly exceeds 15 for the complete sweep of $0.0 \leq \bar{\mu} \leq 0.7$. As seen from Fig. 6, the FEM-M and FEM-D have fast convergence up to $\bar{\mu} = 0.7$ whereas the shooting method exhibits slow convergence for $\bar{\mu} \geq 0.65$. Summarizing, we observe that the FEM-M and FEM-D are much better regarding iteration counter or speed of convergence; at $\bar{\mu} = 0.7$, for example, iteration counter for FEM-M and FEM-D is about 15, whereas it is about 55 for the shooting method, nearly four times higher.

The divergence problem of the Newton iteration due to the starting values is further pursued in Fig. 7 in the ρ-$\bar{\mu}$ plane, where ρ is related to the starting values as starting value = $\rho \times$ exact solution. Here, $\rho = 0.0$ and $\rho = 1.0$ imply that all of the starting values are zero and exact solution, respectively. (The exact solution at any flight speed is that solution obtained by continuation approach with $\Delta\mu = 0.05$.) This is done as a means of quantifying the sensitivity to possible extremes of starting values and of connecting these results with an earlier investigation.[1] The other possibility of large initial values ($\rho > 1$) is not exercised separately. The divergence boundary of Fig. 7 corresponding to the shooting method is similar to that of Ref. 1; the minor differences are due to the sensitivity of these boundaries to discretization in ρ and $\bar{\mu}$. Even with

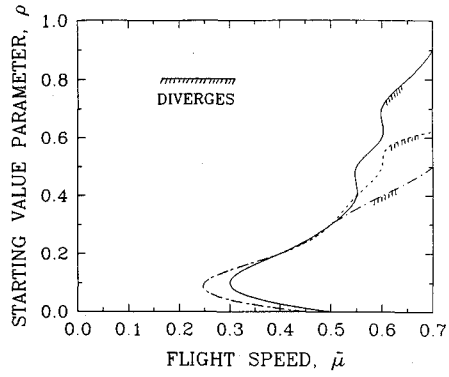

Fig. 7 Divergence boundary of the three trim analysis methods without damped Newton iteration (—— shooting, ---- FEM-D, – · – · – FEM-M; converges everywhere with damped Newton iteration).

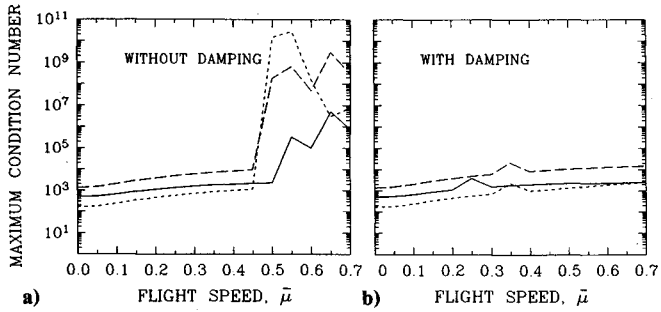

Fig. 8 Effects of damped Newton parameter on the Jacobian matrix condition number in the three trim analysis methods with zero starting values (—— shooting, --- FEM-D, ---- FEM-M).

somewhat improved starting values, say $\rho = 0.1$ compared with $\rho = 0.0$, erratic behavior of the boundaries merits mention. The damped Newton iteration reduces the erratic behavior in general; indeed, in Fig. 7 it converges everywhere. With poor starting values (low values of ρ, say less than 0.5), divergence with Newton iteration is not unexpected since it guarantees only local convergence and is sensitive to starting values anyway. What is unexpected is divergence in the shooting method for ρ as high as 0.8. Concerning divergence boundary, shooting method is affected more than FEM-M and FEM-D. This supports the iteration counter results in Fig. 6.

The unexpected divergence with Newton iteration and the absence of divergence with damped Newton iteration is further investigated in Fig. 8 on the basis of the maximum condition number of the Jacobian matrices of the iterations; see Eqs. (16a) and (16b), respectively. The results are for $\rho = 0.0$, zero starting values. As seen from Fig. 8, the onset of divergence in Fig. 6 for $\bar{\mu} = 0.50$ in the shooting method and $\bar{\mu} = 0.45$ in FEM-M and FEM-D is accompanied by rapid increase in the Jacobian matrix condition numbers for corresponding values of $\bar{\mu}$. By comparison these condition numbers essentially remain constant in all of the three trim analysis methods with damped Newton iteration. This shows that

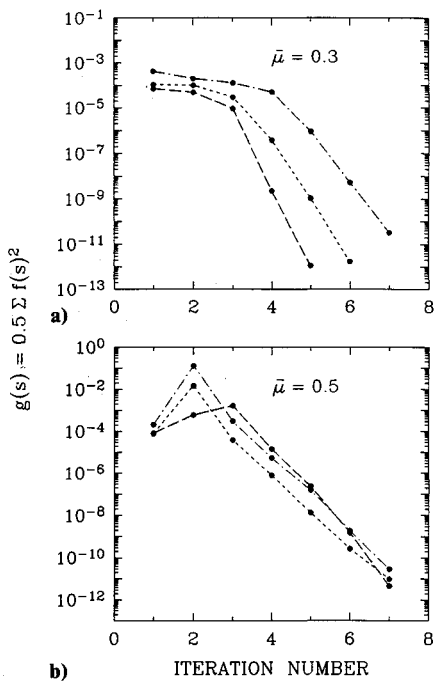

Fig. 9 Minimization of the objective function in the damped Newton iteration in the three trim analysis methods with zero starting values (--- shooting, — · — · — FEM-D, ---- FEM-M).

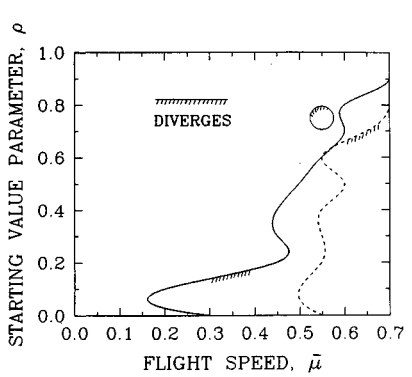

Fig. 10 Divergence boundary of the shooting method with sequential scheme (---- with damping, —— without damping).

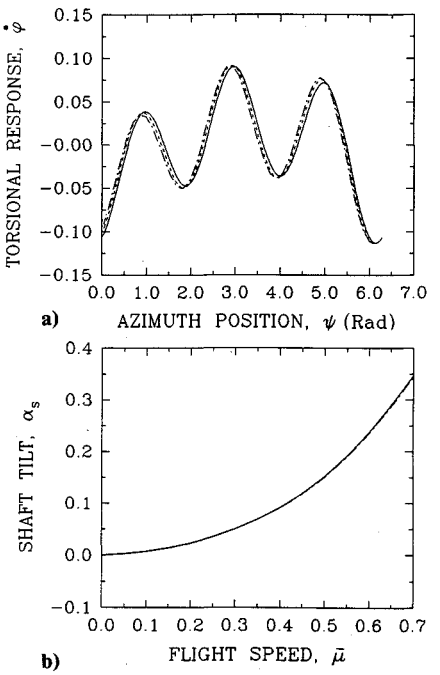

Fig. 11 Comparison of the torsional response and the shaft tilt angle from the three trim analysis methods (—— shooting, ---- FEM-D, — · — · — FEM-M).

damped Newton iteration significantly improves the overall conditioning of the iteration.

Figure 9a shows, for $\bar{\mu} = 0.3$, the monotonic decrease of the objective function; see Eq. (6). We emphasize that $g(s) = 0$ gives the damping parameter λ. It is seen that the objective function decay is monotonic on expected lines in all of the three trim analysis methods and that the minimization is fairly rapid. That is, the iteration counter hardly exceeds seven for $g(s) = 10^{-11}$ for each of the three trim analysis methods. Figure 9b shows the initial nonmonotonic decrease of the objective function. In such cases the algorithm follows the remedial measures referred to earlier in conjunction with Eq. (9). Two distinguishing features of Fig. 9b merit mention. First, even in cases when λ cannot be computed on the basis of monotonic decrease of the objective function, the algorithm still converges to the trim settings with as few as seven iterations in all of the three methods. Second, despite a couple of initial iterations involving nonmonotonic decrease, it later converges with a rapid monotonic decrease.

Thus far, the influence of the damped Newton iteration on the divergence problem of the in-parallel scheme is addressed. We now conclude with a brief discussion of its influence on the sequential scheme. In this scheme, unlike the in-parallel scheme, there are two sets of starting values: one for the response loop and one for the control loop. Without damping, the divergence boundary for the shooting method with the sequential scheme is given in Fig. 10; for the other two methods they remain nearly the same and are not shown. For all the three methods, the starting values for the response loop are assumed zero and those for the control loop are chosen using the starting value parameter ρ—starting value = $\rho \times$ exact control settings—where the exact control settings are those obtained by the continuation approach with $\Delta\bar{\mu} = 0.05$. In this scheme, it is observed that the divergence is mainly due to the sensitivity of the response loop to the physically unrealistic values of the control inputs, estimated in the control loop. When the control-input computations are prevented from generating unrealistically large values either by damping or by a priori stipulation, the response is always found to converge. That is, damping the control loop is more effective than damping the response loop, and therefore, in this illustrative

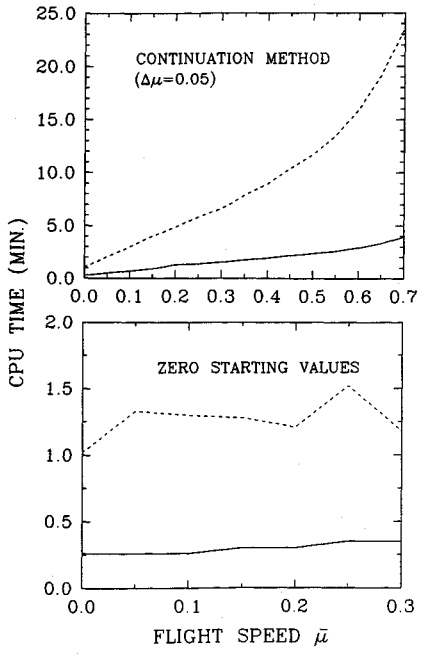

Fig. 12 Machine time comparison in the FEM-D with sequential and in-parallel schemes for flap-lag-torsional model (---- sequential, —— in-parallel).

example, the damped Newton iteration is implemented only in the control loop. After introducing the damped Newton iteration, in both versions of FEM, the sequential scheme converges in the entire ρ-$\bar{\mu}$ plane right up to $\bar{\mu} \leq 0.7$. However, in the shooting method, i.e., Fig. 10, though there is an increase in the region of convergence because of damping the Newton iteration, the iteration was found to cycle for $\bar{\mu}$ beyond 0.55; i.e., after some iterations, the algorithm computes a solution that it has already computed in one of the previous iterations, and hence the algorithm enters into an infinite loop without converging. This cycling phenomenon is found to be independent of the ill-conditioning or near-singularity of the Jacobian as quantified by the condition number of the Jacobian. This problem is involved and not well understood,[10] and there seems to be no known method to treat it effectively.

The preceding investigation based on the flap-lag model results is further verified on the basis of flap-lag-torsion model results. The rotor parameters are identical to those of the flap-lag model; the additional torsional parameters are $\omega_\varphi = 3.0$, $J = 0.002$, and $C_\varphi = -0.02$. Overall, the results are nearly identical to those of the flap-lag model results, specifically these results refer to damped Newton iteration (e.g., divergence boundary, condition number, and monotonic decrease of objective function) and to sequential scheme vis-a-vis in-parallel scheme. In Fig. 11, we select for illustration the torsional response rate $\dot{\varphi}(t)$ among the six components of the state vector $y = \lfloor \beta, \dot{\beta}, \zeta, \dot{\zeta}, \varphi, \dot{\varphi} \rfloor^t$ and the shaft tilt angle α_s among the four components of the control-input vector $c = \lfloor \theta_0, \theta_c, \theta_s, \alpha_s \rfloor^t$. The results from the three methods agree. Finally, as in Figs. 3–5, Fig. 12 shows the machine time saving with the in-parallel scheme in the FEM-D method; similar trends (not shown) are exhibited by the FEM-M and shooting methods with the in-parallel scheme. The only major difference between the flap-lag and flap-lag-torsion results concern NEL or the number of elements needed for asymptotic convergence of the periodic response as shown in Fig. 2. For the latter case, because of the highly oscillatory nature of the torsional response, NEL values as high as 60 and 90 are needed for FEM-D and FEM-M, respectively.[14]

Concluding Remarks

The three trim analysis methods are investigated with an optimally selected damping parameter λ; $\lambda = 1$ refers to conventional Newton iteration. With each trim analysis method, both the sequential and in-parallel schemes of computations of initial conditions and control inputs are exercised. The computational efficiency is described on the basis of both machine time and convergence characteristics, which are quantified by the maximum condition number of the Jacobian matrices of the Newton iteration. The iteration counter and its growth with increasing flight speed and divergence boundaries correlate with this quantification. That investigation demonstrates the feasibility of using an optimally selected Newton damping parameter in the in-parallel scheme to improve the computational efficiency of the trim analysis. It also shows the following:

1) In the three trim analysis methods with both the sequential and in-parallel schemes, the optimally selected damping parameter virtually eliminates divergence up to flight speed $\bar{\mu} = 0.7$ except for a small region beyond $\bar{\mu} > 0.55$ in the shooting method with the sequential scheme.

2) The in-parallel scheme takes much less machine time compared with the sequential scheme with comparable convergence characteristics.

3) At very high advance ratios (for $\bar{\mu} > 0.6$ or so), the shooting method shows slow convergence in that the iteration counter and the machine time increase rapidly. By comparison, FEM-M and FEM-D show fast convergence for the entire range of $0 \leq \bar{\mu} \leq 0.7$.

4) The cycling phenomenon observed at $\bar{\mu} > 0.55$ in the shooting method with the sequential scheme and with damped Newton iteration merits further research.

The preceding investigation is restricted to a generic Newton-Raphson iteration and does not consider a wide class of related methods such as the quasi-Newton and other globally convergent methods. Nevertheless it should provide a reference point for using and comparatively assessing such methods in helicopter trim analysis.

Acknowledgments

This work is partially sponsored by the U.S. Army Research Office under Research Grants DAAL03-87-K-0037 and DAAL03-91-G0007 and the Aeroflightdynamics Directorate of the NASA Ames Research Center under Research Grant NAG 2-727. David A. Peters of Washington University took keen interest during the progress of this investigation and offered several comments. We are grateful to him.

References

[1]Peters, D. A., and Izadpanah, A. P., "Helicopter Trim by Periodic Shooting with Newton-Raphson Iteration," 37th Annual Forum of the American Helicopter Society, Paper 23, New Orleans, LA, May 1981.

[2]O'Mally, J. A., III, Izadpanah, A. P., and Peters, D. A., "Comparison of Three Numerical Trim Methods for Rotor Air Loads," Ninth European Rotorcraft Forum, Paper 58, Stresa, Italy, Sept. 1983.

[3]Izadpanah, A. P., "P-Version of Finite Elements for the Space-Time Domain with Application to Floquet Theory," Ph.D. Dissertation, Georgia Inst. of Technology, Atlanta, GA, Aug. 1986, Chap. 3.

[4]Borri, M., "Helicopter Rotor Dynamics by Finite Element Time Approximation," *Computers and Mathematics with Applications,* Vol. 12A, No. 1, 1986, pp. 149–160.

[5]Peters, D. A., and Izadpanah, A. P., "hp-version of Finite Elements for the Space-Time Domain," *Computational Mechanics,* Vol. 3, No. 2, 1988, pp. 73–88.

[6]Bauchau, O. A., and Hong, C. H., "Nonlinear Response and Stability Analysis of Beams Using Finite Element in Time," *AIAA Journal,* Vol. 26, No. 9, 1988, pp. 1135–1142.

[7]Stephens, W. B., Ruthaushi, M. J., Ormiston, R. A., and Tan, C. M., "Development of Second Generation Comprehensive Helicopter Analysis System (2GCHAS)," American Helicopter Society National Specialists' Meeting on Rotorcraft Dynamics, Arlington, TX, Nov. 1989.

[8]Hodges, D. H., and Bless, R. B., "A Weak Hamiltonian Finite

Element Method for Optimal Control Problems," *Journal of Guidance, Control, and Dynamics,* Vol. 14, No. 1, 1991, pp. 148–156.

[9]Hodges, D. H., and Hou, L. J., "Shape Functions for Mixed p-Version Finite Elements in the Time Domain," *Journal of Sound and Vibration,* Vol. 145, No. 2, 1991, pp. 169–178.

[10]Ascher, U. M., Mattheij, R. M. M., and Russell, R. D., *Numerical Solution of Boundary Value Problems for Ordinary Differential Equations,* Prentice-Hall, Englewood Cliffs, NJ, 1988, pp. 327–357.

[11]Bertsekas, P. D., *Constrained Optimization and Lagrange Multiplier Methods,* Academic Press, New York, 1982, Chap. 1.

[12]Ortega, J. M., *Numerical Analysis; A Second Course,* Academic Press, New York, 1972, Chap. 2.

[13]Ravichandran, S., Gaonkar, G. H., Nagabhushanam, J., and Reddy, T. S. R., "A Study of Symbolic Processing and Computational Aspects in Helicopter Dynamics," *Journal of Sound and Vibration,* Vol. 137, No. 3, 1990, pp. 495–507.

[14]Achar, N. S., "Trim Analysis by Shooting and Finite Elements and Floquet Eigenanalysis by QR and Subspace Iterations in Helicopter Dynamics," Ph.D. Dissertation, Florida Atlantic Univ., Boca Raton, FL, April 1992, Chap. 4.